EFFECT OF CHEMICAL COMPOSITION AND SUPERHEAT ON MACROSTRUCTURE OF HIGH Cr WHITE IRON CASTINGS

Ö.N. Doğan
Albany Research Center
U.S. Department of Energy, U.S.A.
e-mail: dogano@alrc.doe.gov

ABSTRACT

White cast irons are frequently used in applications requiring high wear resistance. High Cr white cast irons have a composite microstructure composed of hard $(Fe,Cr)_7C_3$ carbides in a steel matrix. Previous research has indicated that the equiaxed region of these high Cr white iron castings is much more wear resistant under high stress abrasive conditions than the columnar region, when the carbides are oriented perpendicular to the wear surface. In the present study, the effect of both the chemical composition, particularly carbon content, and the pouring superheat of the melt on the macrostructure of high Cr white iron castings is investigated.

Keywords: white cast iron, chemical composition, wear

1. INTRODUCTION

White cast irons are frequently used in applications requiring high wear resistance. High Cr white cast irons have a composite microstructure composed of hard $(Fe,Cr)_7C_3$ carbides in a steel matrix. In thick section castings, long rod-shaped carbides may grow perpendicular to the mold wall to form the columnar zone of the casting, or their long axes may grow in random directions to form equiaxed grains. Previous research has indicated that the equiaxed region of these high Cr white iron castings is much more wear resistant under high stress abrasive conditions than the columnar region, when the carbides are oriented perpendicular to the wear surface [1,2]. Therefore, in order to maximize their abrasion resistance, it is essential that wear resistant cast parts with thick sections be produced with completely equiaxed macrostructures to maximize their abrasion resistance. In the present study, the effect of both the chemical composition, particularly carbon content, and the pouring superheat of the melt on the macrostructure of high Cr white iron castings is investigated.

2. EXPERIMENTAL PROCEDURE

Hypoeutectic, eutectic, and hypereutectic compositions of each of two high Cr white cast irons, containing 15 and 26 weight percent Cr, were melted in an induction furnace and poured into chemically bonded sand molds to produce 5cmx5cmx18cm bars. Two pouring temperatures for each alloy were used. The chemical compositions and the superheats of the castings are listed in Table 1. The superheats were calculated by subtracting the solidification start temperature, as determined by differential thermal analyses, from the pouring temperature. The chemistry of the melts was determined by atomic absorption spectroscopy and a combustion-infra-red detection technique. The solidification macrostructures were observed on the fracture surfaces of the cast bars. The microstructures of polished surfaces were characterized using both reflected light optical microscopy and scanning electron microscopy.

Table 1. Chemical composition (in weight percent) and pouring superheat of castings.

Alloy	Cr	C	Ni	Si	Mn	Fe	Superheat (ºC)	
							Low	High
Hypo15Cr	15.2	3.5	0.18	0.51	0.61	Balance	90	265
Eutec15Cr	15.1	3.7	0.22	0.43	0.55	Balance	110	285
Hyper15Cr	15.3	4.3	0.13	0.65	0.55	Balance	65	315
Hypo26Cr	26.2	2.8	0.38	0.42	0.93	Balance	90	265
Eutec26Cr	26.2	3.1	0.28	0.43	1.02	Balance	60	235
Hyper26Cr	26.0	3.7	0.22	0.79	0.92	Balance	90	265

Differential thermal analyses (DTA) were performed on an instrument fitted with a pair of matched alumina crucibles with tantalum lids. One crucible contained the sample with a mass of between 50 and 100 mg, while the other was empty. After evacuation of the DTA chamber, a flow of 1.67 cm^3/s of high purity argon was maintained throughout the experiment. Specimens were heated to 50ºC above the liquidus temperature at 5ºC/min, allowed to equilibrate for 5 min, and then cooled at 5ºC/min to 700ºC. The temperature difference between the crucibles was monitored during heating and cooling. Heat taken up or given up during the analysis was plotted after normalizing for a 100 mg sample weight.

3. RESULTS AND DISCUSSION

3.1 MICROSTRUCTURE

The cast microstructures of the 26Cr alloy are shown in Figure 1. The hypoeutectic 26Cr alloy contains proeutectic austenite dendrites and eutectic cells composed of M_7C_3 carbides and austenite (Figure 1a). The austenite dendrites in the low-superheat casting are finer than those observed in the casting with high superheat. M_7C_3 carbides with both rod type and blade type morphology are observed, regardless of superheat temperature. The microstructure of the eutectic 26Cr alloy, on the other hand, is composed completely of eutectic cells ($\gamma + M_7C_3$), as shown in Figure 1b. On average, the carbide size is the finest in the eutectic alloys, and the carbide morphology is completely rod type. When viewed perpendicular to their growth direction, the M_7C_3 carbides in the eutectic cells are very fine in the center of the cells, but become coarser with increased distance from the center. Finally, in the hypereutectic 26Cr alloy (Figure 1c), large proeutectic M_7C_3 carbides predominate, with eutectic cells ($\gamma + M_7C_3$) comprising the rest of the microstructure. The carbides in the hypereutectic 26Cr alloy are principally blade-like, although some rod-like carbides are also observed. The blade-like eutectic carbides are most apparent adjacent to the large proeutectic M_7C_3 carbides.

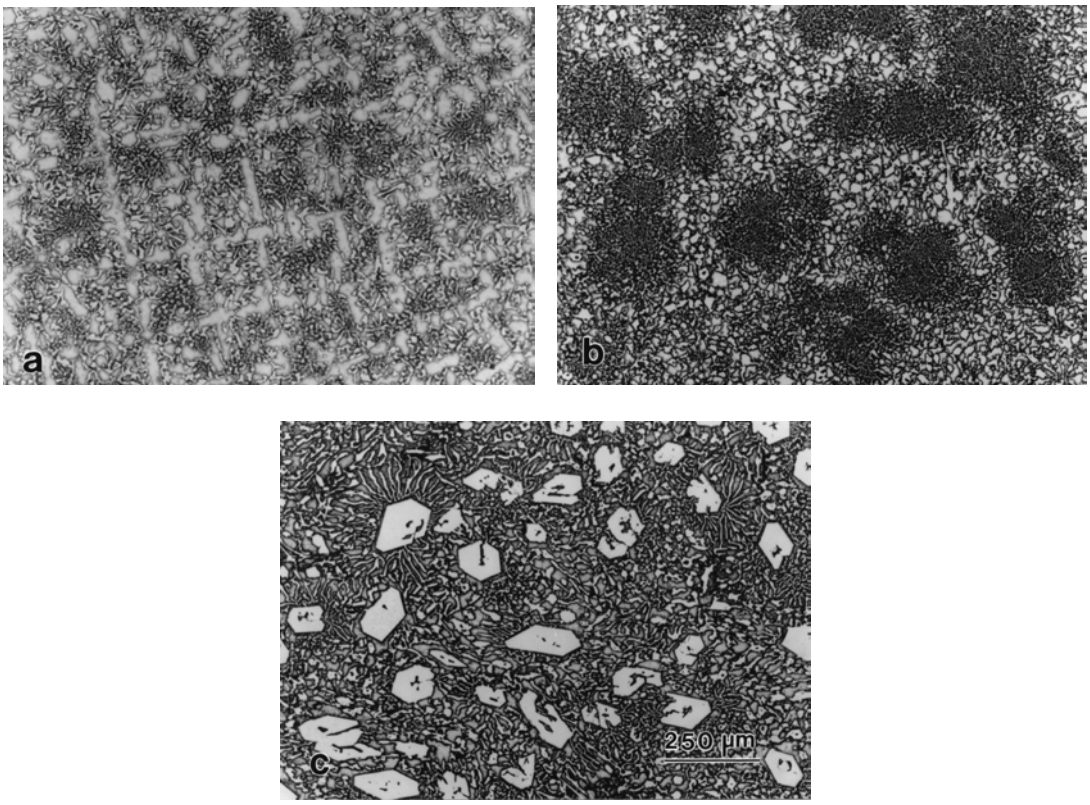

Fig.1 - Optical micrographs of the 26Cr alloys poured with high superheats: (a) hypoeutectic, (b) eutectic, (c) hypereutectic. Etched with Vilella's reagent.

The 15Cr alloys have carbide microstructures similar to their counterparts in the 26Cr series; however, the matrix is different (Figure 2). The matrix of the 15Cr alloys solidifies as austenite, but transforms primarily to bainite (with some to pearlite) during cooling. Prior austenite dendrites, observed primarily as bainite, and eutectic cells composed of bainite and M_7C_3, form the microstructure of the hypoeutectic 15Cr alloy. The eutectic 15Cr alloy contains eutectic cells in which the austenite has transformed to bainite and pearlite. As in the eutectic 26Cr alloy, the carbides are finer at the center of the eutectic cells and coarser at the outer regions of the cells, indicating that eutectic solidification begins in the center of the cell at a certain undercooling and proceeds radially outward. As solidification progresses, the undercooling decreases due to the latent heat released; consequently, the carbides forming later during solidification are coarser.

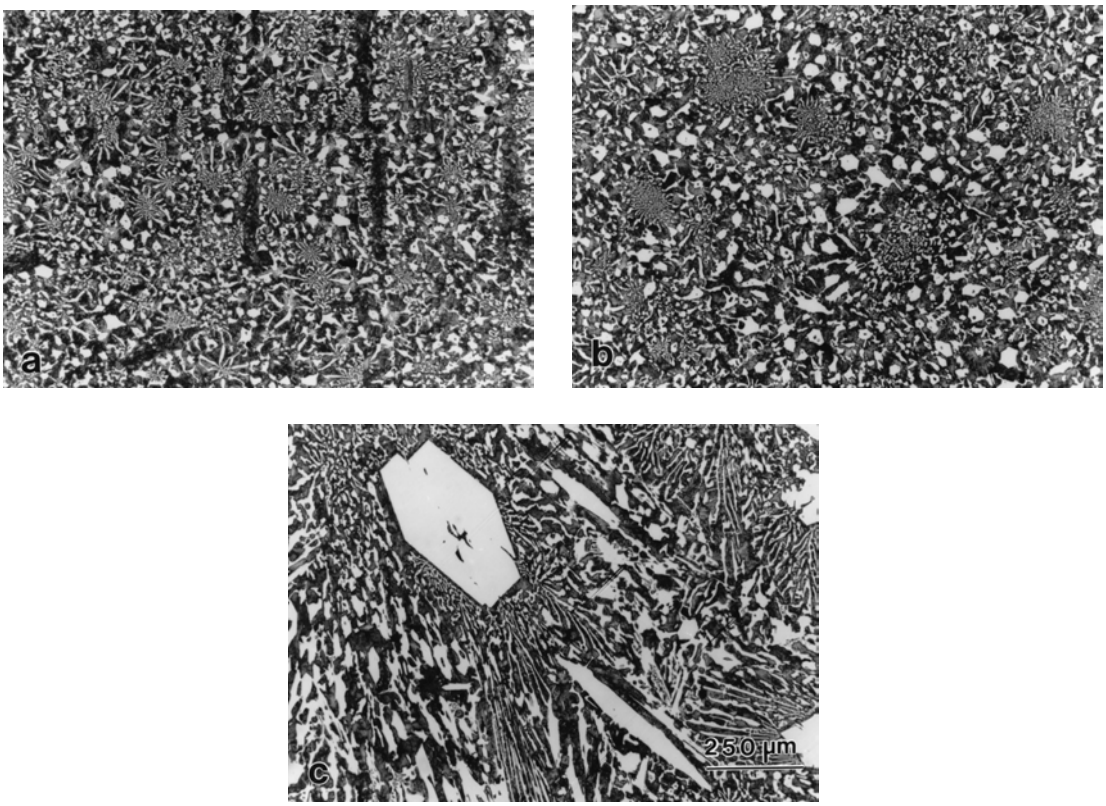

Fig.2 - Optical micrographs of the 15Cr alloys poured with high superheats: (a) hypoeutectic, (b) eutectic, (c) hypereutectic. Etched with Vilella's reagent

The hypereutectic 15Cr alloy is characterized by very large proeutectic M_7C_3 carbides with eutectic cells filling the space between them. The blade morphology of eutectic carbides is more dominant in the hypereutectic 15Cr alloy than in the hypereutectic 26Cr alloy. In addition, in the hypereutectic 15Cr alloy, a peritectic M_3C phase and a binary eutectic Fe_3C

are also observed, as illustrated in the backscattered electron micrograph in Figure 3. The core and rim structure forms in these carbides because the M_3C phase is a product of the reaction between the remaining liquid and the previously solidified eutectic M_7C_3 carbides [3-6]. The large proeutectic M_7C_3 carbides do not react with the remaining liquid to produce a core and rim structure since their surroundings are already solid before the peritectic reaction temperature is reached. In other words, they act as effective nucleation points for the eutectic reaction ($L \rightarrow \gamma + M_7C_3$).

From the results of this study, it is clear that the carbides in these alloys may have one of two morphologies: rod or blade. While the 15Cr eutectic and 26Cr eutectic alloys contain completely rod-type M_7C_3 carbides, the hypoeutectic and hypereutectic alloys have both rod- and blade-type carbides. In the hypereutectic alloys, the proeutectic M_7C_3 carbides are always rod shaped. Subsequent solidification around the proeutectic carbides results in the formation of blade type carbides. This morphology suggests that when the undercooling is smaller (because of the heat released by the formation of the proeutectic M_7C_3 carbides), the blade-like carbide shape is favored. Similarly, the microstructure of the hypereutectic 26Cr casting in regions near the mold wall, where the undercooling is larger, typically contains many more rod-shaped carbides (Figure 4) than the interior of the casting (Figure 1c). This relationship between undercooling and carbide morphology also explains why there is higher proportion of blade-like carbides in the hypoeutectic alloys. In this case, the undercooling is reduced by the latent heat released by the solidification of austenite. These observations support earlier studies [7-10], which argued that slower growth rates favor a blade-like carbide morphology, whereas faster growth rates favor a rod-like carbide shape in different eutectic systems.

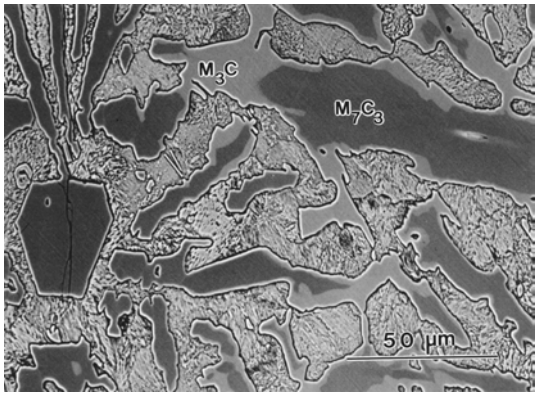

Fig.3 - Backscattered electron micrograph illustrating the product of the peritectic reaction ($L + M_7C_3 \rightarrow M_3C$) in the hypereutectic 15Cr alloy.

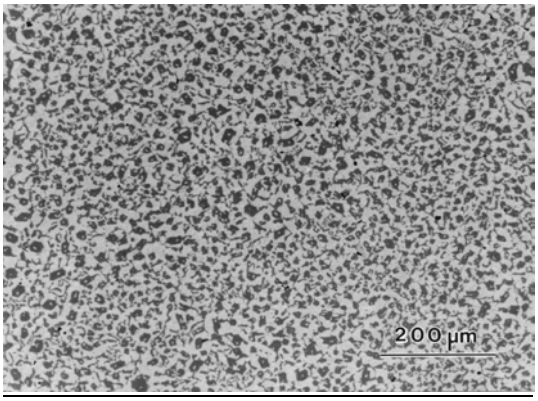

Fig.4 - Backscattered electron image showing uniformly distributed carbide rods very near the mold wall in the hypereutectic 26Cr casting.

3.2 MACROSTRUCTURE AND THERMAL ANALYSIS

The solidification macrostructures of the castings vary significantly with both the chemical composition and the pouring temperature (superheat). Figures 5 shows this variation for the 26Cr alloy. In both the 15Cr and 26Cr alloys, high superheats produce completely columnar structures. Earlier investigations [11-14] have explained the relationship between superheat and the columnar/equiaxed transition. At high superheats, the grains that form due to contact with cold surfaces during pouring, and which might serve as nuclei for the formation of equiaxed grains, remelt, and the columnar grains growing inward from the mold/molten metal interface take up all the space.

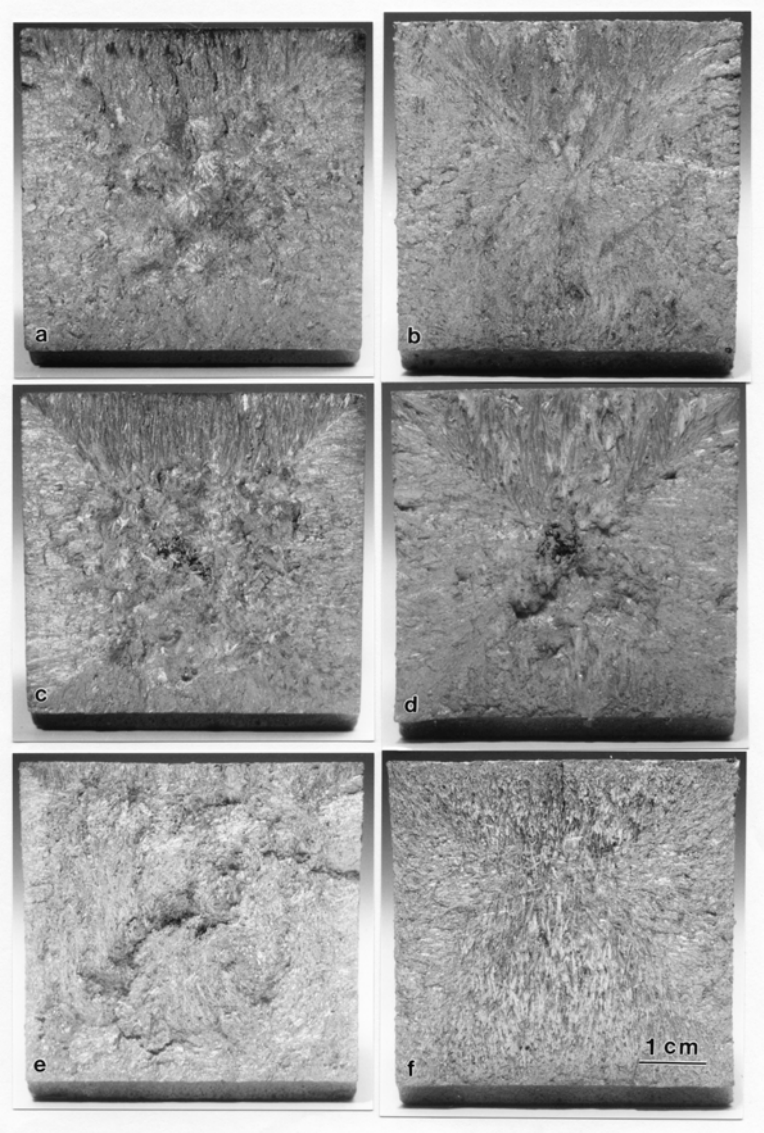

Fig.5 - Solidification macrostructure of the 26Cr castings as seen on the fracture surfaces: (a) hypoeutectic alloy with a low superheat, (b) hypoeutectic alloy with a high superheat, (c) eutectic alloy with a low superheat, (d) eutectic alloy with a high superheat, (e) hypereutectic alloy with a low superheat, and (f) hypereutectic alloy with a high superheat.

At low superheats, the hypoeutectic and the eutectic alloys contain similar volume fractions of columnar and equiaxed grains. In the hypereutectic compositions, on the other hand, at superheats of 65 and 90□C, the cast structure is composed almost completely of equiaxed grains, with only a thin chill layer near the mold wall. This suggests that the primary carbides which form first during solidification of the hypereutectic alloys, are more effective nuclei for the eutectic phase than the proeutectic austenite dendrites in the hypoeutectic alloy.

The results of DTA runs of the hypereutectic alloys and the hypoeutectic 26Cr alloy are shown in Figures 6-8. The upper curves on these diagrams are the heating curves and the lower curves are the cooling curves. The heating curve for the hypereutectic 15Cr alloy consist of a large endothermic peak between 1157 and 1215°C and a broad endotherm between 1215 and 1280°C (Figure 6). The area under the large peak represents the heat taken up due to the melting of matrix and some of the eutectic carbides. The area under the broad curve represents the heat taken up due to the dissolution of primary carbides into the melt. From the shape of this curve, one can conclude that the kinetics of the dissolution reaction is slow compared to those of the preceding reaction. The first reaction to occur during the cooling of the hypereutectic 15Cr melt is the formation of primary M_7C_3 carbides at about 1257°C. This reaction continues until the monovariant eutectic reaction ($L \rightarrow \gamma + M_7C_3$) begins at 1200°C. After the eutectic reaction, a monovariant peritectic reaction ($L + M_7C_3 \rightarrow M_3C$) occurs at about 1195°C, followed by another monovariant eutectic reaction ($L \rightarrow \gamma + M_3C$) at about 1172°C, and finally a binary eutectic reaction ($L \rightarrow \gamma + Fe_3C$) at about 1142°C. Similar reactions are observed in the DTA curves of the hypereutectic 26Cr alloy (Figure 7) with the exeptions that all the reactions are shifted to higher temperatures and that the lower temperature reactions which are observed during the cooling of the 15Cr alloy do not occur.

The phase transformations observed by DTA also occur when a melt with a similar composition is poured into a sand mold. As a result, the features observed on the heating and cooling DTA curves can be utilized to design the final macrostructure of casting. In this respect, the three important features of the heating and the cooling DTA curves are (*i*) the broadness of the M_7C_3 dissolution reaction during heating, indicating slow dissolution kinetics; (*ii*) the temperature difference between the high temperature end of the M_7C_3 dissolution curve during heating and the start temperature of primary M_7C_3 formation during cooling; and (*iii*) the approximately 60°C temperature difference between the start temperature for the primary M_7C_3 reaction and the start temperature for the eutectic reaction ($L \rightarrow \gamma + M_7C_3$).

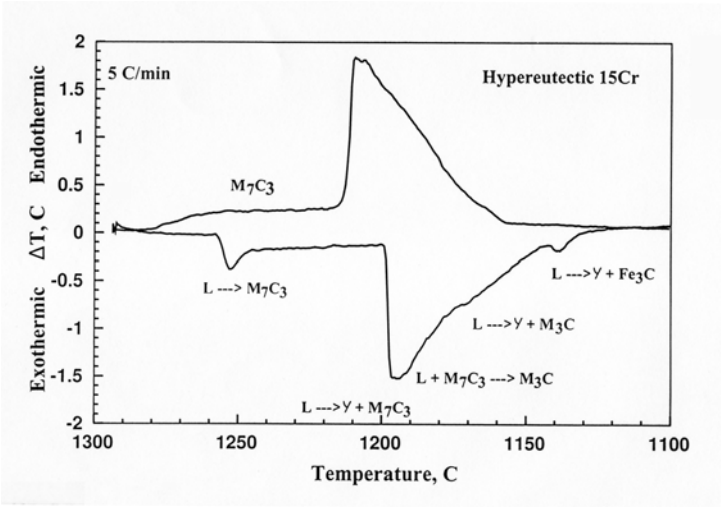

Fig.6 - DTA curves showing the reactions taking place during heating and cooling of hypereutectic 15Cr alloy.

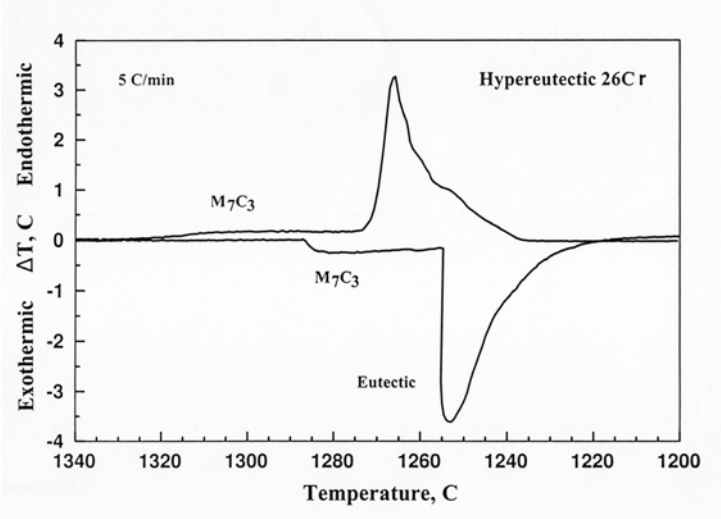

Fig.7 - DTA curves showing the reactions taking place during heating and cooling of hypereutectic 26Cr alloy.

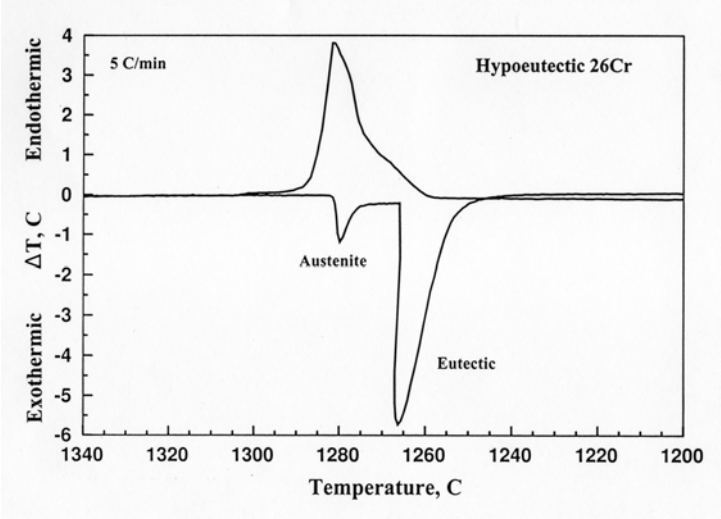

Fig.8 - DTA curves showing the reactions taking place during heating and cooling of hypoeutectic 26Cr alloy.

When a moderately superheated (50-100°C), hypereutectic melt is poured into a cold sand mold, that part of the melt which contacts the cold surfaces of the runner and mold cavity begins to freeze. In the hypereutectic composition, the first phase to form is the primary M_7C_3 particles. The frozen particles are transported freely with the flow into the mold cavity due to the large temperature difference (about 60°C in the 15Cr alloy) between primary carbide formation and the eutectic reaction. Once the M_7C_3 precipitates form, the decreasing superheat of the bulk melt may not be sufficient to completely dissolve them. In addition, even if the M_7C_3 particles are heated to their dissolution temperature by the remaining superheat of the melt, they may not have enough time to dissolve in the melt due to their slow dissolution kinetics. These primary M_7C_3 particles in the melt act as nucleation sites for the equiaxed grains of the subsequent eutectic solidification.

This observation is contrary to a previous study [15], which found that M_7C_3 is not an effective nucleant for austenite in a high purity Fe-Cr-C alloy. This contradiction may be in part due to the fact that commercial grade compositions were used in the present study. Powell and Randle [16] recently found that there is a strong orientation relationship between the carbides and the austenite phase in a high purity Fe-Cr-C alloy, resulting in a distinct texture in the solidification structure. However, they did not observe a similar texture in a commercial grade high Cr white cast iron containing 1.3 wt% Si. These observations support the idea that the ease of austenite nucleation is strongly dependent upon the composition of the melt.

From these results, it can be concluded that the slow dissolution kinetics of M_7C_3 in the melt, combined with the temperature gap between the beginning of the formation of proeutectic M_7C_3 during solidification and the end of the dissolution reaction for M_7C_3 during melting, can be exploited to obtain a completely equiaxed macrostructure using a slightly hypereutectic Fe-Cr-C melt and a pouring temperature with a low superheat.

The aforementioned phenomena cannot take place in the hypoeutectic alloys, because the primary phase to form in these alloys is austenite, which melts first during heating, as shown in the DTA diagram in Figure 8. The inefficiency of the austenite phase to act as nuclei for the eutectic phase is also apparent in the fact that the equiaxed zone is approximately the same size in both the hypoeutectic and eutectic alloys at low superheats. In the eutectic alloys, this process, of course, would not happen since there is only one reaction taking place during solidification.

4. CONCLUSIONS

1. A completely equiaxed cast macrostructure can be obtained using a slightly hypereutectic high Cr white iron melt with a low superheat.
2. Slower growth rates favor blade-like carbide morphology, whereas faster growth rates favor rod-like carbide shape in high Cr white irons.

5. REFERENCES

1. Ö.N. DOĞAN, G. LAIRD II, AND J.A. HAWK, *Wear*, 181-183, 342, (1995).
2. Ö.N. DOĞAN AND J.A. HAWK, *Wear*, 189, 136, (1995).
3. C.P. TONG, T. SUZUKI, AND T. UMEDA, *Physical Metallurgy of Cast Iron IV*, Proceedings of the Fourth International Symposium, Eds. G. Ohira, T. Kusakawa, and E. Niyama, p. 403, Materials Research Society, Pittsburgh, PA, (1990).
4. G. LAIRD II, R.L. NIELSEN, AND N.H. MACMILLAN, *Metall. Trans. A*, 22, 1709, (1991).
5. V. RANDLE AND G. LAIRD II, *J. Mater. Sci*., 28, 4245, (1993).
6. W.R. THORPE AND B.CHICCO, *Mater. Sci. Eng.*, 51, 11, (1981).
7. H.B. SMARTT, AND T.H. COURTNEY, *Metall. Trans. A*, 3A, 2000-2002 (1972).
8. F.D. LEMKEY, R.W. HERTZBERG, AND J.A. FORD, *Trans. The Metall. Soc. AIME*, 233, 334-341, (1965).
9. D. JAFFREY AND G.A. CHADWICK, *Trans. The Metall. Soc. AIME*, 245, 2435-2440, (1969).
10. G.L.F. POWELL, *Metals Forum*, 3, 37-46, (1980).
11. B. CHALMERS, *Principles of Solidification*, p.255, Robert A. Krieger Publishing Company, Inc., Malabar, FL, (1982).
12. R. MORANDO, H.BILONI, G.S. COLE, AND G.F. BOLLING, *Metall. Trans. A*, 1, 1407, (1970).
13. G.S. COLE AND G.F. BOLLING, *Trans. The Metall. Soc. AIME*, 245, 725, (1969).
14. A. OHNO, *Solidification-The Separation Theory and Its Applications*, Springer-Verlag, Berlin (1987).
15. G.L.F. POWELL, *Materials Transactions, JIM*, 31, 110, (1990).
16. G.L.F. POWELL AND V. RANDLE, *J. Materials Sci*., 32, 561-565 (1997).